Received: 22 February 2023 | Accepted: 4 July 2023

DOI: 10.1111/1462-2920.16464

BRIEF REPORT

ENVIRONMENTAL MICROBIOLOGY Applied Microbiology International

Respiratory protein interactions in *Dehalobacter* sp. strain 8M revealed through genomic and native proteomic analyses

Jesica M. Soder-Walz[1] | **Kenneth Wasmund**[2,3] | **Darja Deobald**[4] | **Teresa Vicent**[1] | **Lorenz Adrian**[4,5] | **Ernest Marco-Urrea**[1]

[1]Departament d'Enginyeria Química, Biològica i Ambiental, Universitat Autònoma de Barcelona (UAB), Bellaterra, Spain

[2]Division of Microbial Ecology, Centre for Microbiology and Environmental Systems Science, University of Vienna, Vienna, Austria

[3]School of Biological Sciences, University of Portsmouth, Portsmouth, UK

[4]Department Environmental Biotechnology, Helmholtz Centre for Environmental Research—UFZ, Leipzig, Germany

[5]Chair of Geobiotechnology, Technische Universität Berlin, Berlin, Germany

Correspondence
Lorenz Adrian, Department Environmental Biotechnology, Helmholtz Centre for Environmental Research—UFZ, Permoserstraße 15, 04318 Leipzig, Germany.
Email: lorenz.adrian@ufz.de

Funding information
European Regional Development Fund; Generalitat de Catalunya, Consolidated Research Group, Grant/Award Number: 2021-SGR-01008; Spanish Ministry of Economy and Competitiveness State Research Agency, Grant/Award Number: PID2019-103989RB-I00

Abstract

Dehalobacter (*Firmicutes*) encompass obligate organohalide-respiring bacteria used for bioremediation of groundwater contaminated with halogenated organics. Various aspects of their biochemistry remain unknown, including the identities and interactions of respiratory proteins. Here, we sequenced the genome of *Dehalobacter* sp. strain 8M and analysed its protein expression. Strain 8M encodes 22 reductive dehalogenase homologous (RdhA) proteins. RdhA D8M_v2_40029 (TmrA) was among the two most abundant proteins during growth with trichloromethane and 1,1,2-trichloroethane. To examine interactions of respiratory proteins, we used blue native gel electrophoresis together with dehalogenation activity tests and mass spectrometry. The highest activities were found in gel slices with the highest abundance of TmrA. Protein distributions across gel lanes provided biochemical evidence that the large and small subunits of the membrane-bound [NiFe] uptake hydrogenase (HupL and HupS) interacted strongly and that HupL/S interacted weakly with RdhA. Moreover, the interaction of RdhB and membrane-bound *b*-type cytochrome HupC was detected. RdhC proteins, often encoded in *rdh* operons but without described function, migrated in a protein complex not associated with HupL/S or RdhA. This study provides the first biochemical evidence of respiratory protein interactions in *Dehalobacter*, discusses implications for the respiratory architecture and advances the molecular comprehension of this unique respiratory chain.

INTRODUCTION

Organohalides are frequently found as pollutants in the environment. Although some organohalides are naturally generated, their presence in groundwater is due to their wide use in industrial processes followed by improper management and accidental spills. Trichloromethane (TCM) and 1,1,2-trichloroethane (1,1,2-TCA) are among those of environmental concern and are ranked 11 and 170 on the 2022 Agency for Toxic Substances and Disease Registry Priority List of Hazardous Substances, respectively, based on a combination of the frequency of their detection, toxicity and potential for human exposure (ATSDR, 2022).

Bioremediation using organohalide-respiring bacteria (OHRB) is a feasible and low-cost strategy to treat contaminated groundwater (Blázquez-Pallí et al., 2019; Jugder et al., 2016). OHRB are anaerobic microorganisms characterized by their ability to gain energy for growth by using halogenated compounds as terminal

electron acceptors, yielding less-halogenated compounds as products (Wang et al., 2018). Reductive dehalogenase homologous (RdhA) are the enzymes responsible for reductive dehalogenation and usually contain two iron–sulfur clusters and a corrinoid cofactor (Hug et al., 2013; Kräutler et al., 2003). To date, anaerobic respiratory dechlorination of TCM has been found only in bacteria of the genera *Dehalobacter* and *Desulfitobacterium*. Characterized TCM-dechlorinating RdhA proteins include CtrA (Ding et al., 2014), ThmA (Zhao et al., 2017), TmrA (Wong et al., 2016) and CfrA (Tang & Edwards, 2013). All these RdhA proteins except for ThmA are also active against 1,1,2-TCA. DcrA has dechlorination activity with both 1,1-dichloroethane and 1,1,2-TCA (Tang & Edwards, 2013).

Most RdhA proteins are produced with an N-terminal twin-arginine leader (TAT) peptide that targets them for export through the cytoplasmic membrane. After cleavage of the TAT-leader peptide, they keep attached to the cytoplasmic membrane presumably by interaction with the integral membrane protein RdhB. Other proteins involved in the flow of electrons between hydrogenases and RdhA have been studied, but their role is not fully understood. Recent studies provided direct biochemical evidence that quinone-independent respiration in *Dehalococcoides* and *Dehalogenimonas* depends on the presence of a large membrane-bound protein complex (Kublik et al., 2016; Seidel et al., 2018; Trueba-Santiso et al., 2021). In addition to the RdhA and RdhB proteins, this respiratory complex contains the three canonical subunits of a complex iron–sulfur molybdoenzyme with the molybdopterin-binding subunit OmeA (potentially also having an iron–sulfur cluster), a four iron–sulfur cluster protein HupX and multiple transmembrane domains containing integral membrane protein OmeB (Rothery et al., 2008) and the two subunits of hydrogen (H_2) uptake hydrogenase (HupL and HupS; Seidel et al., 2018; Trueba-Santiso et al., 2021).

A tentative model for the respiratory chain in the *Dehalobacter* genus has been proposed for *Dehalobacter restrictus* strain PER-K23 based on biochemical, genomic and proteomic data and consisted of H_2 uptake by a cytochrome *b* containing Hup-type [NiFe]-hydrogenase (HupA [=HupS], HupB [=HupL] and HupC), which was described to transfer electrons to menaquinone. From the reduced menaquinone (menaquinol) electrons are described to be transferred to halogenated compounds via RdhA (Maillard & Holliger, 2016). In strain PER-K23, tetrachloroethene (PCE) reductive dehalogenase (PceA) and its membrane anchor PceB are encoded in the genome as part of a four-gene cluster (*pceABCT*), which is a unique characteristic of the genera *Dehalobacter* and *Desulfitobacterium* compared to other OHRB (Duret et al., 2012). PceT is predicted to function as a molecular chaperone assisting in the folding of PceA (Maillard et al., 2011). PceC was believed to encode a putative transcriptional regulator in *Desulfitobacterium hafniense* strain Y51 (Jugder et al., 2015), although recently it has been tentatively proposed to form a membrane-bound protein with PceA and PceB with a role in the electron chain based on the predicted redox activity of a flavin mononucleotide (FMN)-binding domain in *Des. hafniense* (Buttet et al., 2018). A recent study using quantitative proteomics found a similar abundance of PceA and PceB, suggesting they could form protein complexes in *Deh. restrictus* strain PER-K23 and *Des. hafniense* strain TCE1, but PceC was not present in the complex (Cimmino et al., 2022). In conclusion, the function of RdhC in *Dehalobacter*, which is homologous to PceC, is unclear.

Previous work in our laboratory focused on the enrichment of a *Dehalobacter*-containing culture from TCM-contaminated groundwater samples (Soder-Walz et al., 2022). The 16S rRNA gene sequence of the dominant *Dehalobacter* strain was 99.66% similar to the 16S rRNA gene sequence of *Deh. restrictus* strain PER-K23, and it was denominated *Dehalobacter* sp. strain 8M (Soder-Walz et al., 2022). The strain 8M enrichment completely transformed TCM to dichloromethane (DCM) and 1,1,2-TCA to a mixture of vinyl chloride (VC) and 1,2-dichloroethane (1,2-DCA). Compound-specific isotope analysis revealed significant differences in both carbon and chlorine isotope effects during dechlorination of TCM by our *Dehalobacter* sp. strain 8M enrichment compared to other *Dehalobacter*-containing enrichments (Heckel et al., 2019; Soder-Walz et al., 2022). This phenomenon has recently been attributed to amino acid differences in the vicinity of the active site of the TCM-transforming RdhA (Phillips et al., 2022).

Here, we report the analysis of the genome of the *Dehalobacter* sp. strain 8M and its proteome profile during growth with TCM and 1,1,2-TCA. We also combined blue native polyacrylamide gel electrophoresis (BNE), dehalogenation activity assays and protein mass spectrometry to provide biochemical evidence of the molecular organization of the respiratory chain of this *Dehalobacter* strain, together with the identification of the RdhA involved during growth with TCM and 1,1,2-TCA.

EXPERIMENTAL PROCEDURES

Chemicals and cultivation

All chemicals used were of the highest available purity (Supporting Information Materials and Methods S1).

Dehalobacter sp. strain 8M was grown in 100-mL glass serum bottles with 65 mL of an anoxic defined medium containing 0.2 g L^{-1} potassium dihydrogen phosphate, 0.27 g L^{-1} ammonium chloride, 1 g L^{-1}

sodium chloride, 0.41 g L^{-1} magnesium chloride hexahydrate, 0.52 g L^{-1} potassium chloride, 0.15 g L^{-1} calcium chloride dihydrate and 0.25 mg L^{-1} resazurin as redox indicator. The following trace elements were added: 0.7 mg L^{-1} zinc chloride, 0.8 mg L^{-1} manganese (II) chloride tetrahydrate, 0.06 mg L^{-1} boric acid, 0.19 mg L^{-1} cobalt (II) chloride hexahydrate, 0.02 mg L^{-1} copper (II) chloride dihydrate, 0.24 mg L^{-1} nickel (II) chloride hexahydrate, 0.36 mg L^{-1} sodium molybdenum oxide dihydrate, 20 mg L^{-1} iron (II) chloride tetrahydrate, 128 mg L^{-1} nitrilotriacetic acid, 0.02 mg L^{-1} sodium tungstate dihydrate, 0.015 mg L^{-1} sodium selenite and 0.68 g L^{-1} sodium acetate as carbon source. The culture medium was aliquoted in serum bottles inside an anaerobic glovebox, closed with Teflon-coated butyl rubber stoppers and aluminium crimp caps and autoclaved at 121°C for 30 min. Once autoclaved and cooled, the following components were added under anoxic and sterile conditions: 0.7 g L^{-1} sodium bicarbonate to buffer the pH at 7.0, 24 mg L^{-1} $Na_2S{\cdot}9H_2O$ and 48 mg L^{-1} L-cysteine as reducing agents, 0.2 g L^{-1} yeast extract and a vitamin solution containing: 5 μg L^{-1} D-(+)-biotin, 25 μg L^{-1} calcium D-(+)-pantothenate, 50 μg L^{-1} thiamine hydrochloride, 20 μg L^{-1} 4-aminobenzoic acid, 50 μg L^{-1} nicotinic acid, 75 μg L^{-1} pyridoxine hydrochloride and 50 μg L^{-1} cyanocobalamin. TCM or 1,1,2-TCA was added with a syringe through the septum as electron acceptor and the cultures were gassed with H_2 to 0.4 bar overpressure, supplied as electron donor. All bottles were incubated statically in the dark at 25°C. The final pH of the medium was 7.0. During the exponential growth phase and when accompanied by an exponential increase of organohalide transformation, active cultures were transferred into fresh medium (4.3% v/v inoculum) prior to the amendment of H_2. All experiments were performed using cultures growing for more than five transfers with the same electron acceptor. Abiotic controls without inoculum were included in triplicate to evaluate abiotic transformation.

Gas chromatography

Organohalide compounds were quantified using an Agilent 6890 N gas chromatograph with a flame ionization detector, equipped with a DB-624 column (30 m length, 0.32 mm inner diameter with 0.25 mm film thickness) by injecting 0.5 mL headspace samples, as described previously (Trueba-Santiso et al., 2017). Data acquisition and peak integration were performed using Chromeleon 6.8 Chromatography Software (Dionex Corporation). The results are expressed as nominal concentrations, which correct for headspace-liquid partitioning equilibrium within the bottle. Calibration was based on aqueous standards, with the same liquid and headspace volumes as in the microcosms.

Metagenome sequencing and analysis

A volume of 700 mL fully grown culture liquid that had transformed approximately 2100 μmol TCM (3000 μM) was centrifuged at 8000*g* for 40 min at 16°C to collect cells. Half of the supernatant was removed and discarded, and the remaining volume was centrifuged again. This process was repeated three times and the resulting cell pellet was washed once with 1 mL of sterile 100 mM phosphate buffer (pH 7.2). Finally, the cells were suspended in 1 mL of sterile 100 mM phosphate buffer (pH 7.2). Genomic DNA was extracted with the Gentra Puregene Yeast/Bact kit (Qiagen) following the manufacturer's instructions.

DNA was sequenced in 2 × 150 bp paired-end mode using a HiSeq 3000 (Illumina) at the Biomedical Sequencing Facility, Vienna. Sequence reads used for genome assembly were trimmed of adapters using AdapterRemoval with default settings (Schubert et al., 2016). Sequence reads were also trimmed based on quality using a python3 script (https://github.com/kwasmund/Trim-Illumina), with the following flags -q 15 -m 50 –b 8. Sequences were assembled using SPAdes (v. 3.10.1) with pre-assembly read-error correction (Bankevich et al., 2012). Contigs <5000 bp were discarded. Contigs that were more or less than 60–65× coverage were also discarded, because BLASTX analyses against the National Center for Biotechnology Information (NCBI) nr database identified that contigs with this coverage all belonged to *Dehalobacter*.

The genome sequence was automatically annotated using the RAST server using 'classic mode' (Aziz et al., 2008) and also using the MAGE MicroScope pipeline (Vallenet et al., 2020). The loci numbers used in this manuscript are from the MicroScope annotation and are preceded by the letters 'D8M_v2_'. The JspeciesWS website (Richter et al., 2016) was used to calculate the average nucleotide identities (ANI) of genomes by BLASTn. Genome quality was evaluated with CheckM (Parks et al., 2015).

Protein biochemistry

Cells for whole-cell proteomic analysis were harvested from biological triplicate samples of 140 mL each upon the consumption of 2500 μM of TCM or 1,1,2-TCA. The cultures were repeatedly centrifuged at 8000*g* for 40 min at 16°C and only half of the supernatant was removed per centrifuge cycle to avoid the loss of cells. The procedure was repeated three times and 4 mL cell concentrates were obtained (resulting in a 35-fold concentration) for each electron acceptor. Cell concentrates were disrupted by the freeze–thaw method (−80°C/+40°C repeated five times), followed by sonication for 30 s. Amicon ultrafilters with an exclusion size of 10 kDa were employed to concentrate the

samples (Amicon Ultra, 0.5 mL Centrifugal Filters, Millipore) by centrifuging at 4°C for 30 min at 14,000*g*. The concentrated proteins were recovered by turning the filters upside down and centrifuging for 2 min at 1000*g* and 4°C. Disulfide bridges in the protein samples were reduced with dithiothreitol and cysteine residues were alkylated with iodoacetamide prior to digestion with 0.6 μg of porcine trypsin at 37°C overnight. The reaction was stopped with 0.1% (final concentration) formic acid. The extracted peptides were desalted using C_{18} Zip Tip columns for further analysis by nano-liquid chromatography–tandem mass spectrometry (nLC-MS/MS; Seidel et al., 2018).

For analysis of protein complexes by BNE, cells were harvested as described above by centrifugation of 210 mL of cultures that had consumed 2000 μM of TCM or 1,1,2-TCA. This resulted in a cell concentrate with about 10^{10} cells mL^{-1}, as determined by epifluorescence microscopic cell counting on agarose-coated slides (Adrian et al., 2007). The cells were disrupted by bead beating (Fast Prep FP120, Thermo) in six cycles of 40 s at 4 m s^{-1}, alternating with 1 min on ice. Membrane proteins were solubilized with 0.1% *n*-dodecyl-D-maltoside under gentle shaking on ice for 1 h. The solubilized protein extract was recovered as supernatant from a centrifugation step at 14,000*g* for 15 min at 4°C. This supernatant was filtered with a 0.22 μm filter (Millipore) to remove cell debris.

Inside the anaerobic chamber, a 4–16% gradient Bis-Tris gel (NativePAGE Novex, Invitrogen) was loaded with 25 μL per well of protein extract amended with 0.125% w/v Coomassie G-250 additive. NativeMark Unstained Protein Standard (Invitrogen) was used as the protein ladder. Anode buffer and light blue cathode buffer required for the electrophoresis run were prepared according to the manufacturer's instructions, degassed and chilled to 4°C before their use. The electrophoresis was run at 150 V for 1 h and the voltage was then raised to 250 V for 30 min. The BNE system was kept cold by using ice packs during the run.

After the electrophoresis run, two replicate lanes with cell extract and one lane with the protein ladder were separated from the rest of the gel and these three lanes were silver-stained with a mass-spectrometry compatible procedure (Kublik et al., 2016). Further four replicate lanes with cell extract were not stained and were kept cold and wetted with anode buffer until they were cut into slices using a scalpel that was cleaned after each cut. The cuts were guided by the bands observed in the parallel silver-stained lanes. The cut-out unstained gel slices were placed into individual 10-mL glass vials to perform activity assays (see below). The two stained gel lanes were used to identify proteins in the visible bands by protein mass spectrometry. For that, the two stained lanes were cut into slices of equal size for subsequent in-gel trypsin digest (see below). The BNE gel lane prepared from the culture grown with TCM was cut into 20 slices; the lane prepared from 1,1,2-TCA was cut into 18 slices.

For dehalogenase activity assays, the dechlorinating activity was quantified in cell suspensions and gel slices of the BNE. In both cases, the experiments were set up inside the anaerobic chamber using 10-mL glass vials, with 2 mL (final volume) of a reaction mix containing 200 mM potassium acetate buffer (pH 5.8), 2 mM methyl viologen as electron donor and 2 mM titanium (III) citrate [2 mM in respect to titanium (III)] as reducing agent, cell concentrate or a gel slice and finally amended with 300 μM of TCM or 300 μM of 1,1,2-TCA from 0.6 M acetonic stock solutions. The resulting acetone concentration in the assays was 6.4 mM, which did not prevent the transformation of halogenated compounds.

For assays with cell suspensions, 200 μL of a cell concentrate (10^8–10^9 cells mL^{-1}) harvested from the TCM dechlorinating culture were added to each vial and triplicate samples were incubated with TCM or 1,1,2-TCA, separately. Correspondingly, the same procedure was performed with the culture grown with 1,1,2-TCA, although in this case, the cellular density was lower (10^7–10^8 cells mL^{-1}).

Dehalogenase activity assayed in gel slices from the BNE of both cultures grown with TCM and 1,1,2-TCA was performed with four non-stained lanes from each gel. After cutting the slices of the BNE as described above, two unstained lanes were incubated with TCM and the other two with 1,1,2-TCA. The gel slices were smashed into small pieces with a scalpel inside the vials. The vials were sealed with Teflon-coated rubber septa and aluminium crimps and amended with the corresponding electron acceptor using a glass syringe (Hamilton).

For all dehalogenase activity assays performed, controls were added in triplicates. Abiotic controls consisted of 2 mL of the reaction mix amended with 300 μM of TCM or 1,1,2-TCA, without adding cells or gel slices. In the case of the activity assays performed with the gel slices, two additional controls were included: (i) the positive control consisted of 25 μL of the protein extract instead of the gel slices incubated with the reaction mix and (ii) the negative control consisted of the remaining pellet after membrane protein solubilization incubated with the reaction mix to assess the performance of the solubilization protocol.

Finally, the vials were vortexed and incubated upside down in the dark, at 25°C shaking at 150 rpm. After 24 h, gas chromatography was used to analyse the transformation of TCM or 1,1,2-TCA and the production of DCM or 1,2-DCA and VC, respectively. The activity in each experimental vial was expressed as the percentage of chlorinated substrate that was transformed into product(s) after 24 h of incubation compared to the initial amount of substrate added to each vial.

For in-gel trypsin digestion and protein mass spectrometry, duplicate silver-stained slices from BNE gels were cut into slices as described above for activity assays, washed with ddH_2O and de-stained in a 1:1 (v/v) solution containing 30 mM $K_3[Fe(CN)_6]$ and 100 mM $Na_2O_3S_2$. Then, the proteins in the gel slices were reduced with dithiothreitol, their cysteine residues were carbamidylated with iodoacetamide and trypsin digested. The resulting peptides were extracted from the gel pieces and desalted as described previously (Vallenet et al., 2020). Extracted peptide samples obtained after in-solution or in-gel digestion were analysed by nLC-MS/MS on a nanoUPLC system (nanoAcquity, Waters) coupled to an Orbitrap Fusion mass spectrometer (Thermo Scientific) as described previously (Seidel et al., 2018). Proteome Discoverer (v2.2, Thermo Fisher Scientific) was used for the identification of proteins, based on a protein database from the draft genome of *Dehalobacter* sp. strain 8M using SequestHT as a search engine. A false discovery rate threshold of 1% was set for peptide identification using the Target Decoy PSM Validator node. The Minora node in Proteome Discoverer was used to quantify the abundance of proteins using label-free quantification based on intensity values in precursor scans. The relative protein abundance presented in this study is the ratio of a protein abundance in one slice to its overall abundance across all slices of one blue native gel lane. The hierarchical cluster analysis was performed with RStudio software using R programming language, applying *hcluster* using default settings (complete linkage) and plotted with *ggplot* to the relative abundance of all proteins detected in one gel lane.

Protein structure prediction and visualization

Multiple sequence alignment of RdhC homologues from different bacteria were calculated with MEGA11 using an implemented MUSCLE algorithm with default settings (Tamura et al., 2021). Signal peptide sequences were identified using SignalP 6.0 (Teufel et al., 2022). Protein structure prediction of RdhC 40031 of *Dehalobacter* sp. strain 8M was conducted with ColabFold (Mirdita et al., 2022). Protein homology was detected by HMM-HMM comparison using the HHpred server of MPI Bioinformatics Toolkit (Zimmermann et al., 2018) and with Conserved Domain Architecture Retrieval Tool (Geer et al., 2002) of the NCBI (Sayers et al., 2022). Cofactor binding sites were predicted with the COFACTOR server (Zhang et al., 2017) and MetalPredator server (Valasatava et al., 2016). Structure modelling, refinement and alignment of RdhC and NqrC subunit of the sodium (Na^+)-translocating NADH:ubiquinone oxidoreductase protein complex from *Vibrio cholerae* were done with PyMOL 2.5.4 (Schrödinger & DeLano, 2020).

Phylogenetic analysis of RdhA

Phylogenetic analysis of RdhA sequences was performed with the Maximum Likelihood algorithm via IQ-TREE by W-IQ-TREE (Trifinopoulos et al., 2016). We included the reference sequences set described by (Hug et al., 2013) and selected reference sequences obtained from the NCBI Genbank database from the best BLASTP hits to proteins of interest, that is, *Dehalobacter* sp. 8M proteins 40029 (TmrA) and 260094. Sequences were aligned using MUSCLE (Edgar, 2004), and the TAT signal peptide sequences were removed after the sequences were aligned. The automatic substitution model finder was used and resulted in the best-fit model being PMB + F + I + G4. Bootstrapping was done with 1000 replications.

RESULTS

General features of the genome and proteomic analysis

The sequenced genome of *Dehalobacter* sp. strain 8M consists of 3,194,592 bp within 62 contigs with an average GC content of 44.5%, and it contains 3400 predicted protein-coding genes. No plasmids were identified. CheckM analysis indicated that the genome was 99.4% complete with 0.8% contamination. The genome of strain 8M is similar to *Deh. restrictus* strain PER-K23, *Dehalobacter* sp. strain TeCB1 and *Dehalobacter* sp. strain E1, sharing 98.72%, 98.70% and 98.13% average nucleotide identities, respectively (Table S1). The average nucleotide identities between strain 8M and the two TCM-dechlorinating *Dehalobacter* strains UNSWDHB and CF were 94.84% and 94.53%, respectively.

We compared the gene annotations of strain 8M for selected pathways and proteins with six available genomes of *Dehalobacter* sp. strains and examined which proteins were expressed in triplicate cultures of strain 8M grown either with TCM or 1,1,2-TCA. The shotgun proteomic analysis of strain 8M identified the expression of a total of 1014 proteins, which represented 29.8% of the annotated proteins (Table S2). The MicroScope gene locus tag prefix 'D8M_v2_' will be omitted in the following sections when referring to specific genes.

The genome contained 22 putative reductive dehalogenases homologous (*rdhA*) genes, genes for 20 putative membrane-anchoring proteins (*rdhB*; Hölscher et al., 2004; Hug et al., 2013), 5 *rdhC* genes (homologues to *Deh. restrictus pceC*; Buttet et al., 2018) and 2 genes for the molecular chaperone (*rdhT*; Table S3). Of the 22 *rdhA* genes, 18 appear to encode for full-length RdhA proteins of 375–512 amino acids including an N-terminal TAT-leader peptide

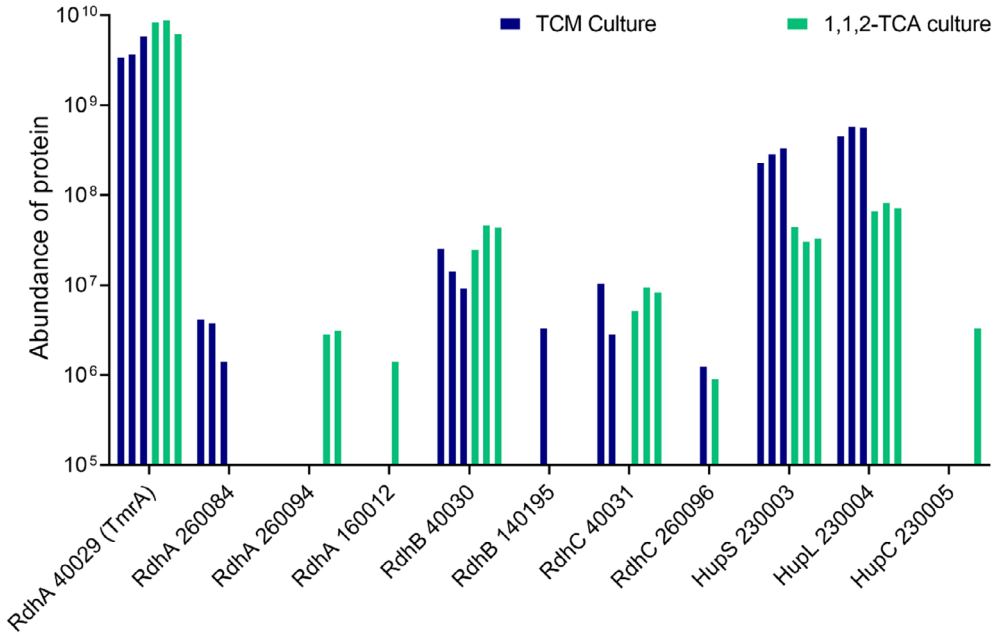

FIGURE 1 RdhA, RdhB, RdhC and HupS, HupL and HupC proteins were detected in full protein extracts of *Dehalobacter* sp. strain 8M grown with TCM or 1,1,2-TCA as only electron acceptors. The data were extracted from the proteomic analyses shown in Table S2. Cultures grown with TCM are represented in dark blue and cultures grown with 1,1,2-TCA in watery green. HupC, b-type cytochrome; HupS, hydrogenase small subunit; HupL, hydrogenase large subunit; RdhA, reductive dehalogenase homologous; RdhB, reductive dehalogenase anchor protein; RdhC, reductive dehalogenase probable membrane associated redox protein; TCM, trichloromethane; 1,1,2-TCA, 1,1,2-trichloroethane.

(RRXFXK) and two FeS cluster binding motifs ($CX_2CX_2CX_3CP$ and $CX_{10\text{-}12}CX_2CX_3CP$; Table S3); in none of the 18 sequences we detected a corrinoid-binding site starting in between the two FeS cluster binding motifs, as described for few other reductive dehalogenases in *Dehalococcoides* strains $DXHX_2G\text{-}X_{50}\text{-}SXL\text{-}X_{42}\text{-}GG$ and $DHXG\text{-}X_{39}\text{-}S\text{-}X_{32}\text{-}G$ (Hölscher et al., 2004; Padilla-Crespo et al., 2014). In contrast, we identified similar motifs downstream of the second FeS cluster binding motifs in 17 of the 18 full RdhA sequences ($WXHX_2G/V/A\text{-}X_n\text{-}FGYG$) but the amino acid residues of these motifs are located far away from the corrinoid in the model structure; therefore they might fulfil other functions than corrinoid-binding. Four *rdhA* genes were fragments of the N-terminal (20015) or C-terminal side (20010, 170062, 550001) but the fragmentation of *rdhA* 20015 and 550001 were artefacts of assembly breaks as they were the last and first open reading frames in a contig, respectively. Of the 20 *rdhB* genes, 19 appear to encode functional RdhB proteins with a length of 100–105 amino acids (1 exception of 91 amino acids) and three transmembrane domains each. The *rdhB* gene 30067 is shorter and would result in an RdhB protein fragment of 60 amino acids and two transmembrane helices. Of the five *rdhC* genes, one (600005) was fragmented due to its position at the end of a contig and was very similar to the N-terminus of RdhC 20012, both containing an N-terminal transmembrane helix. The four full-length RdhC proteins were predicted to be integral membrane proteins with 5–7 transmembrane domains and a length of around 400 amino acids. The detailed analysis of the RdhC structure is described in the last chapter of the 'Results' section.

Shotgun proteomic analysis of strain 8M revealed the expression of two RdhAs in the cultures grown with TCM (40029 and 260084) and three RdhAs in the cultures grown with 1,1,2-TCA (40029, 160012 and 260094; Figure 1). RdhA 40029 was expressed three orders of magnitude higher than the second most abundant reductive dehalogenase, and it was ranked first and second relative to all proteins expressed in the cultures grown with TCM and 1,1,2-TCA, respectively (Table S2). To test the substrate specificity of the detected RdhAs, cell suspensions of cultures grown on TCM or 1,1,2-TCA were used to perform independent enzymatic assays with both substrates as putative electron acceptors. Enzymatic assays with cells grown with TCM almost completely dechlorinated both substrates (94.4 ± 4.8% for TCM and 100% for 1,1,2-TCA) and the dechlorination products generated showed almost stoichiometric conversion to the identified products (90.7 ± 2.8% DCM when the substrate was TCM and 91.3 ± 4.7% 1,2-DCA + VC when the substrate was 1,1,2-TCA; Figure S1). In enzymatic assays with cells grown with 1,1,2-TCA, TCM and 1,1,2-TCA were also quantitatively converted to their respective metabolites but with a lower dechlorination

activity (5.6 ± 2.7% for TCM and 9.8 ± 3.0% for 1,1,2-TCA; Figure S1).

Phylogenetic analysis of RdhA protein sequences of *Dehalobacter* sp. strain 8M showed that the RdhA 40029 affiliated directly with a cluster of known TCM and 1,1,2-TCA dechlorinating RdhA enzymes (Figure S2). Together these form 'orthologue group 46' (all with >90% identity to each other; Hug et al., 2013; Yang et al., 2020). Based on all these characteristics we named RdhA 40029 'TmrA', according to the first RdhA protein in orthologue group 46 described to transform TCM and 1,1,2-TCA (Wong et al., 2016). RdhA 260094 clustered in the vicinity of the orthologue group 46, but is distinct and most similar to several uncharacterized RdhA proteins. The RdhA 260084 is not related to any TCM or 1,1,2-TCA dechlorinating RdhA.

RdhB 40030 and RdhC 40031 that are co-located in one operon with RdhA 40029 were detected in all cultures grown either with TCM or 1,1,2-TCA. In addition, the RdhB 140195 was detected in one replicate of the cultures grown with TCM, and the RdhC 260096 was detected in one replicate in cultures grown with TCM and 1,1,2-TCA (Tables S2 and S3 and Figure 1).

Other genes encoding key metabolic functions, and their protein expression, are described in detail in the Supporting Information and summarized here: For carbon metabolism, the genome of strain 8M encodes and expresses a complete Wood–Ljungdahl pathway and pyruvate: ferredoxin oxidoreductase. Genes for biosynthesis pathways for key co-factors including menaquinone, riboflavin, tetrahydrofolate, pantothenate, CoA, cobalamin, NAD, pyridoxal phosphate and haeme are fully or mostly encoded. For haeme biosynthesis, the classical bacterial pathway is absent, but the sirohaeme-dependent route described in some sulfate-reducing bacteria and archaea is encoded (Layer, 2021). Genes for biotin biosynthesis are not encoded but the genes for a biotin transporter are present. Genes for ubiquinone biosynthesis are not encoded in the genome (Table S4). Corrinoids are essential cofactors for reductive dehalogenases. The genome encodes a complete set of corrinoid biosynthesis enzymes in both, the upper pathway (from glutamyl-tRNA to cobyrinate) and the lower pathway. In contrast to *Deh. restrictus* strain PER-K23, the genome of strain 8M contains an intact *cbiH* gene (170131) that could confer the capacity of growth without the external addition of cobalamin. In strain 8M, 22 of the 24 proteins involved in corrinoid biosynthesis were detected by mass spectrometry in at least one replicate culture, and most of these proteins were detected in all replicates (Table S4). For hydrogen metabolism strain 8M encodes and expresses an outwards-facing membrane-bound three-subunit Hup-type [NiFe] hydrogenase and in addition hydrogenases of the Hyc, Ech and Fe-only type (Table S5).

Interaction of proteins involved in organohalide respiration

In the cultures grown with TCM, the gel lanes were cut into 20 slices, and dechlorinating activity of TCM and 1,1,2-TCA was observed in slices 5–7 and 4–7, respectively (Figures 2A and S3A for the duplicate lanes). Seven different RdhA proteins were detected in the gel slices, but only three of them (40029, 260084 and 260094) were found in both duplicates. The most abundant RdhA was by far TmrA (40029), with the second (260084) and third (260094) RdhA proteins at one and two orders of magnitudes lower, respectively (Table S6). Interestingly, the three most abundant RdhA proteins (TmrA, 260084 and 260094), the hydrogenase subunits HupL (230004) and HupS (230003) and RdhB (260083) showed a similar migration pattern and shared their maximum of relative protein abundance in the slice that showed the highest dechlorinating activity (slice 6, 155 kDa; Figures 2 and S4). The two abundant RdhC proteins (40031 and 260096) showed identical migration patterns and shared their maximum relative protein abundance in slice 7, at 177 kDa. The two membrane subunits HupC (230005) and RdhB (40030) were more broadly distributed between slices 1 to 8 but with a similar migration pattern to each other (Figures 2B and S4B). The RdhAs 20004, 160016 and 140196 had clear maxima at slices 18, 7 and 1, respectively, but they were expressed at a very low abundance and only detected in one single slice which distorted the analysis of relative expression (Figures 2A and S4A and Table S6). All ATP synthase subunits (170067–170072, 170074) shared the same migration pattern and showed a maximum of relative protein abundance in slice 18. The results of protein migration in the duplicate lane are consistent with the described results (Figure S4).

In the cultures grown with 1,1,2-TCA, the gel lanes were cut into 18 slices and the dechlorinating activity of TCM and 1,1,2-TCA was identified in slices 4, 5 and 6 (Figures 2C and S3B). Seven different RdhA proteins were detected in the gels, but the total abundance of RdhA 40029 was between one and four orders of magnitude higher than the second and third most abundant RdhAs 260094 and 160016, respectively (Table S6). The RdhA 40029 had the maximum relative protein abundance in the slices with the highest dechlorination activity of TCM and 1,1,2-TCA in both duplicates (slice 5, 149 kDa), whereas RdhA 260094 had its maximum in a slice that showed high dechlorination activity against 1,1,2-TCA (slice 4, 117 kDa) but only in one of the duplicate samples (Figure S4C). The RdhAs 160016 and 160006 had relative maxima in slices with no dechlorinating activity. As observed in the BNE gels with cell suspensions grown with TCM, HupL (230004) and HupS (230003) co-migrated, with a maximum of

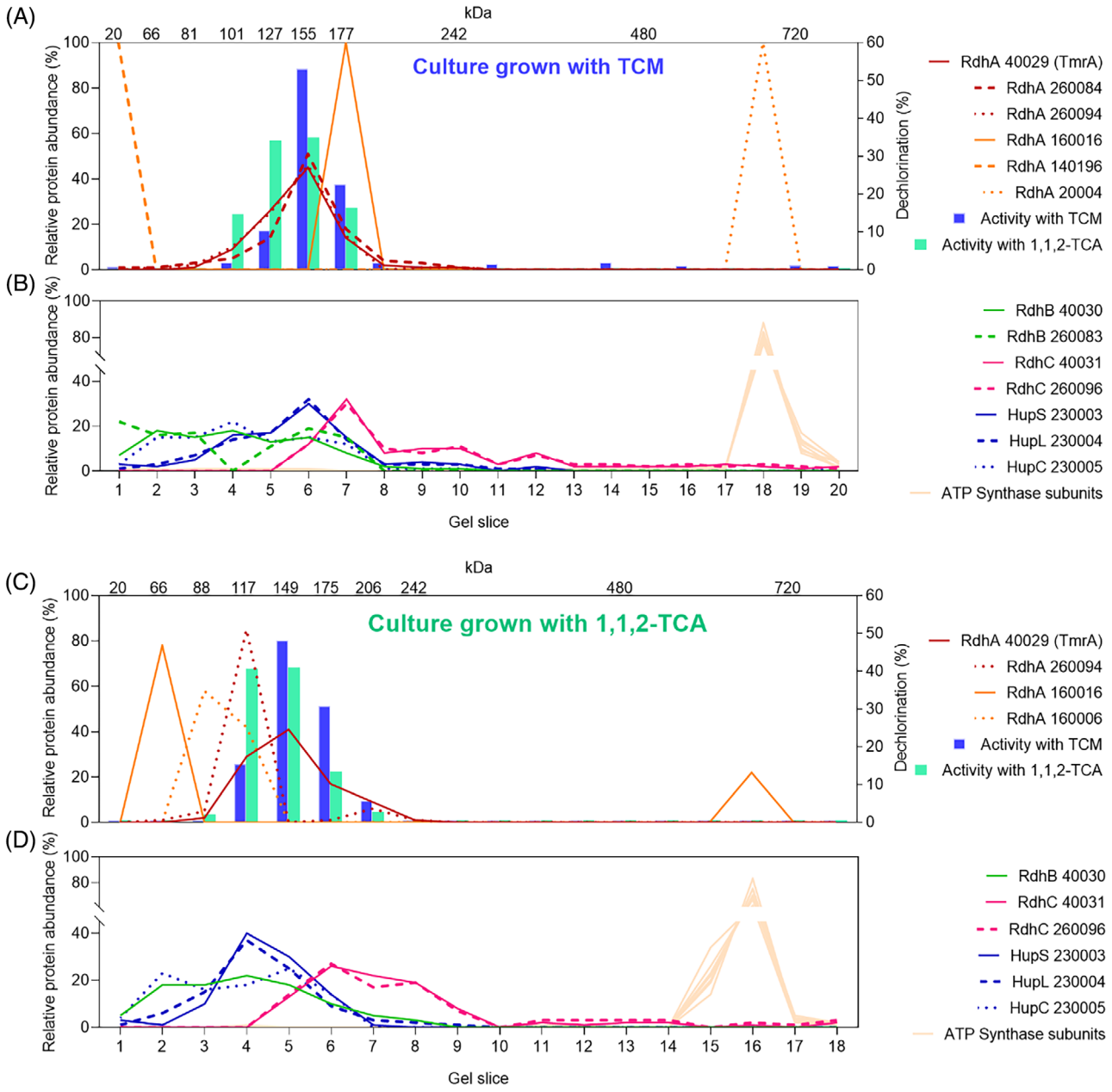

FIGURE 2 TCM and 1,1,2-TCA dechlorination percentages in slices of a BNE gel lane relative to the activity in the whole gel lane (bars), as well as the relative abundance of respiratory proteins throughout the gel lane (lines). (A) Culture grown with TCM as electron acceptor illustrates the reductive dehalogenases and the dechlorinating activity and (B) illustrates the distribution of the remaining respiratory proteins. (C) Culture grown with 1,1,2-TCA as electron acceptor illustrates the reductive dehalogenases and the dechlorinating activity and (D) illustrates the distribution of the remaining respiratory proteins. ATP synthase proteins are shown in the figure in (B) and (D) as a positive control for the extraction and analysis of strongly interacting subunits of a membrane-integrated protein complex. Replicate results are available in Figure S4. BNE, blue native polyacrylamide gel electrophoresis; TCM, trichloromethane; 1,1,2-TCA, 1,1,2-trichloroethane.

relative protein abundance in slice 4, at 117 kDa. The two RdhC 40031 and 260096 also co-migrated and showed their maximum relative protein abundance in slice 6, at 175 kDa, and HupC (230005) and RdhB (40030) were distributed throughout the gel (slices 1–8). All ATP synthase subunits (170067–170072, 170074) shared the same migration pattern and showed a maximum of relative protein abundance in slice 16 (610 kDa). The results of protein migration in the duplicate lanes are very similar (Figure S4).

To identify protein interactions potentially important in organohalide respiration, we performed a hierarchical cluster analysis of the migration patterns and relative abundances of different proteins from all four gel lanes. We also integrated the distribution of the values for the relative activities against TCM and 1,1,2-TCA in

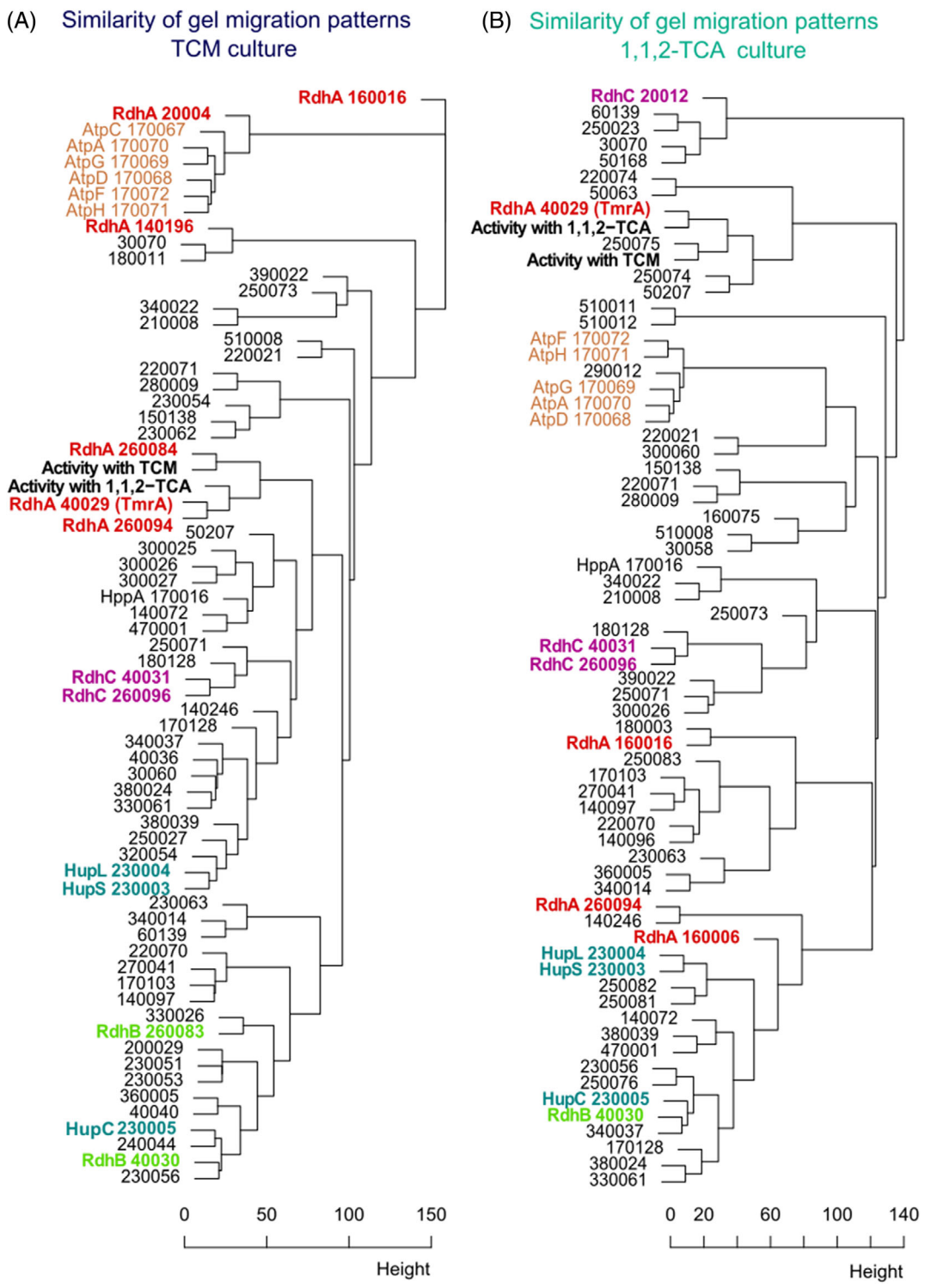

FIGURE 3 Hierarchical cluster analysis of BNE gel migration patterns. Note, this is not a phylogenetic analysis of protein sequences. The graph shows similarities in the migration patterns of the dehalogenating activity (black, bold) and the 60 most abundant proteins plus all RdhA (red), RdhB (green), RdhC (violet), HupS (cyan) and HupC (cyan). The ATPase subunits (ocher) function in the analysis as a positive control to confirm that the cluster analysis of the BNE data shows co-migration of the protein subunits of a larger cluster. (A) Proteins from cultures grown with TCM, (B) proteins from cultures grown with 1,1,2-TCA. Replicates of hierarchical cluster analysis with 60 and 125 most abundant proteins are available in Figures S5 and S6, respectively. BNE, blue native polyacrylamide gel electrophoresis; TCM, trichloromethane; 1,1,2-TCA, 1,1,2-trichloroethane.

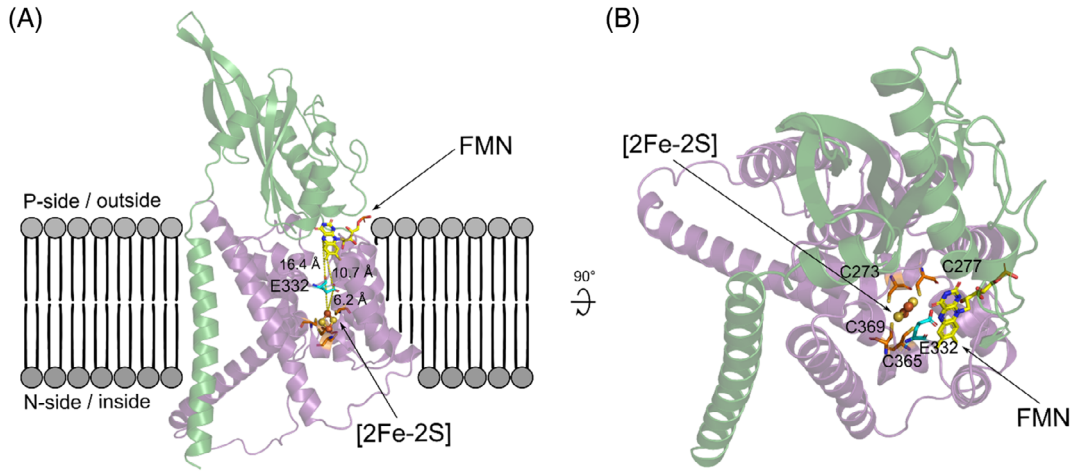

FIGURE 4 AlphaFold2 model of RdhC 40031 from *Dehalobacter* sp. strain 8M. (A) Side view highlighting the seven transmembrane helices. The N-terminal domain of RdhC (in green) is homologous to NqrC and RnfG, has one transmembrane anchor and contains ~150 exoplasmic amino acid residues forming a flavin mononucleotide (FMN)-binding motif. The C-terminal domain of RdhC (in purple) is similar to NapH and NosR and is composed of two transmembrane helix repeats, each bearing two transmembrane helices and a conserved CX_3CP motif. The cysteine residues of the two motifs are highlighted in orange and form a structure potentially complexing a [2Fe-2S] cluster (red and yellow dots) in the middle of the membrane. The glutamic acid residue (E332, cyan stick representation) located between the putative [2Fe-2S] binding site and the FMN (yellow stick representation) might be involved in electron and proton transfer from the cytoplasm through the membrane. Distances are given in Ångstrom (Å). (B) Close-up view from above on the closely aligned sulfhydryl groups of the two CX_3CP motifs oriented towards each other, which putatively coordinate a [2Fe-2S] cluster (red and yellow dots).

this cluster analysis. The dendrograms support that distinct groups of proteins migrate together, regardless of the electron acceptor used: HupL (230004)/HupS (230003), RdhB (40030)/HupC (230005) and RdhC (40031)/RdhC (260096) (Figure 3; Figure S5 shows the distribution in the replica lanes). The clustering of ATP synthase proteins (170067–170072, 170074) indicates they interact with each other forming an independent complex. The two measured activities are tightly co-associated with the most abundant RdhA in each culture. In the cluster analysis of cultures grown with TCM, the TmrA (RdhAs 40029), 260094 and 260084 clusters with both dehalogenating activities in both replicates. In cultures grown with 1,1,2-TCA the activity with TCM tightly co-migrated with TmrA (RdhA 40029) in both replicates but not with other RdhA proteins. The same was observed with the activity against 1,1,2-TCA, except for one replicate that clustered with HupL, HupS, HupC and RdhB. The same three interactions as described above were observed when we performed the hierarchical cluster analysis on the 125 most abundant proteins in a gel lane (Figure S6) or when calculated for all proteins detected (more than 1000 proteins, data not shown).

Structural features of RdhC

The principal architecture of the four full RdhC copies in strain 8M appears to include a single long transmembrane helix at the N-terminus, followed by a long stretch of approximately 150 exoplasmic amino acids and multiple transmembrane domains at the C-terminus. The N-terminal transmembrane helix and the exoplasmic domain of RdhC 40031 harbour a conserved flavin mononucleotide (FMN)-binding domain that is also found in the redox-coupled sodium transporter NqrC of *Vibrio cholerae* (RCSB Protein data bank [PDB] no. 4U9S and 7XK7_C) and RnfG of *Clostridium tetanomorphum* (PDB no. 7ZC6_6) (Buttet et al., 2018). The C-terminal domain of RdhC has no overall strong sequence similarity to known proteins. It includes a duplicated motif with two transmembrane helices each (running through the membrane from the inside to the outside and back), each carrying a highly conserved CX_3CP motif in the cytosolic loop at the end of the two transmembrane helices.

In the AlphaFold2 structural model of RdhC 40031, the N-terminal FMN-binding domain is attached to the membrane via an N-terminal transmembrane helix while the rest of the domain is located outside the cell. In the model, the FMN binding site is located close to the membrane and oriented towards it so that the FMN aromatic rings would be immersed into the membrane (Figure 4A). The two CX_3CP motifs are predicted to be located in the membrane-integrated C-terminal part of RdhC and are arranged three-dimensionally in such a way that they point towards each other giving space to chelate a metal cluster in the middle of the membrane plane (Figure 4B). In the structural model, this metal chelating site is water accessible from the cytoplasmic side and 16.4 Å distant from the FMN molecule. In the middle between the metal chelating site and the FMN molecule, a highly conserved glutamate residue is

located, possibly facilitating electron and/or proton conduction (Figure 4A). For metal cluster prediction, the COFACTOR server predicted no cluster formation with a probability above 1%. In contrast, MetalPredator suggested the formation of a [4Fe-4S] cluster with an e-value of 3.9×10^{-15}.

DISCUSSION

Comparison of the genome of *Dehalobacter* sp. 8M with other *Dehalobacter* genomes

Overall, the genome of strain 8M shares similar functional gene contents with the other six available *Dehalobacter* genomes. Strain 8M possesses a complete set of genes encoding the Wood-Ljungdahl pathway, which is encoded in all *Dehalobacter* strains except for strain EB1. It has been hypothesized that the Wood-Ljungdahl pathway might have another role than CO_2-fixation in *Dehalobacter* strains because strain TeCB1 was isolated and grown in a bicarbonate-free medium (Alfan-Guzman et al., 2017b) and no known *Dehalobacter* isolate was described to grow autotrophically with H_2 and CO_2. The Wood-Ljungdahl pathway in *Dehalobacter* species might operate in the oxidative direction. In this direction, acetate is enzymatically cleaved, resulting in the production of a methyl group and CO. The methyl group is subsequently transferred to tetrahydrofolate, while the electrons generated from the oxidation of CO to CO_2 by carbon monoxide dehydrogenase can be channelled into a reduction pool (Alfan-Guzman et al., 2017b). The corrinoid biosynthesis-associated genes are fully encoded, which is a common feature among *Dehalobacter* strains except for strains PER-K23 and E1 (Rupakula et al., 2013). However, the ability of strain 8M to grow without exogenously supplied cobalamin needs experimental confirmation because the culture medium used contained cyanocobalamin, and the accompanying bacteria might also provide corrinoids. Menaquinone seems to be the only quinone-type electron carrier that could be synthesized by strain 8M, and it could shuttle electrons between [NiFe]-hydrogenase and RdhA as proposed previously for *Deh. restrictus* PER-K23 (Schumacher & Holliger, 1996). Genome analyses further suggest that *Dehalobacter* synthesize haeme via the sirohaeme-dependent pathway, as described for several sulfate-reducing bacteria and archaea (Bali et al., 2011; Kühner et al., 2014; Layer, 2021). This correlates with the presence of cytochrome-encoding genes, for example, *hupC*. In line with other available *Dehalobacter* genomes, the biosynthesis pathway for biotin is missing in strain 8M, suggesting that biotin is required in the medium for growth.

Identification of the RdhA involved in TCM and 1,1,2-TCA dechlorination

TmrA (RdhA 40029) was the first and second most abundant protein in cultures grown with 1,1,2-TCA and TCM, respectively. Interestingly, TmrA was the only reductive dehalogenase expressed in all duplicate cultures grown with either TCM or 1,1,2-TCA in the proteome profile (Figure 1). This protein was also the most abundant RdhA in all BNE gel lanes (Table S6) and had its maximum relative protein abundance in the BNE slices with the highest dechlorinating activity towards TCM and 1,1,2-TCA (Figures 2 and S4). Cluster analyses supported this close association of TmrA with reductive dehalogenase activity. Therefore, our data suggest that TmrA was responsible for the reductive dechlorination of both TCM and 1,1,2-TCA. TmrA displays high amino acid identity with TmrA (97%, EQB22800.1), CfrA (95%, WP_242827270.1), ThmA (95%, ANI21407.1), DcrA (94%, WP_242824980.1) and CtrA (93%, AGO27983.1) from *Dehalobacter* sp. strains UNSWDHB, CF, THM1 and DCA and *Desulfitobacterium* sp. strain PR, respectively (Table S3). Collectively, all these reductive dehalogenases share their ability to dechlorinate TCM, but the RdhA proteins of strains 8M and UNSWDHB differ from the others by their inability to completely (100% of the substrate) transform 1,1-dichloroethane and 1,1,1-trichloroethane (Ding et al., 2014; Soder-Walz et al., 2022; Tang & Edwards, 2013; Wong et al., 2016). Testing of TCM and 1,1,2-TCA transformation in enzymatic assays with cell suspensions of strain 8M showed similar dechlorinating activity for both compounds, regardless of the electron acceptor used to grow strain 8M (Figure S1), which is in agreement with the dechlorination activity of the TCM-dechlorinating RdhA TmrA towards both TCM and 1,1,2-TCA (Jugder et al., 2017).

Although TCM-dechlorinating RdhA proteins share high amino acid sequence similarity, previous studies have shown differences in both carbon and chlorine isotope fractionation during TCM dechlorination by different *Dehalobacter* strains and their associated RdhA, including strain 8M, strain CF (CfrA), UNSWDHB (TmrA) and a RdhA identified in the commercial enrichment culture KB-1 Plus CF (Heckel et al., 2019; Phillips et al., 2022; Soder-Walz et al., 2022; Table S7). This difference in the isotopic pattern has led to questions about the reaction mechanisms of very similar RdhA proteins. In a recent study, Phillips et al. (2022) hypothesized that these differences in carbon and chlorine isotope effects are related to amino acid differences in the active sites of CfrA compared to TmrA and the KB-1 Plus CF RdhA. They proposed that the low C and Cl isotope effects observed in cultures containing TmrA and the KB-1 Plus CF RdhA are associated with the similarity in their amino acid residues Phe80, Phe388

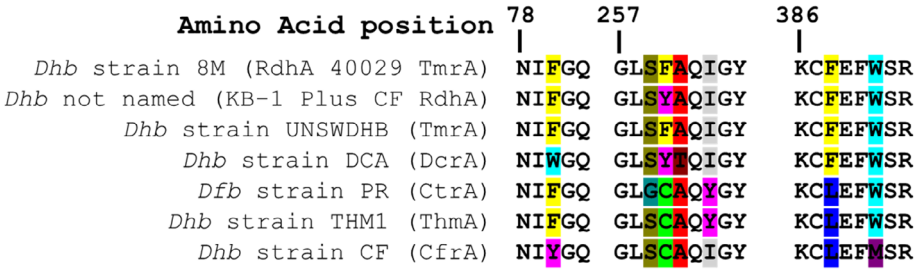

FIGURE 5 Alignment of the RdhA region has been suggested to determine isotopic fractionation of TCM in different OHRBs (Phillips et al., 2022). Highlighted residues indicate differences from the consensus sequence. Alignments were prepared using COBALT software (Papadopoulos & Agarwala, 2007). The enzymes responsible for the TCM transformation are indicated in parenthesis. *Dfb*, *Desulfitobacterium*; *Dhb*, *Dehalobacter*; OHRB, obligate organohalide-respiring bacteria; TCM, trichloromethane.

and Trp391. The influence of these three amino acids on the isotopic fractionation pattern observed on C and Cl isotope effects is further supported by the identification of TmrA and its amino acid sequence in this study since TmrA displayed the same amino acid residues at positions 80, 388 and 391 as the RdhA proteins TmrA and KB-1 Plus CF (Figure 5) and had the same low carbon and chloride enrichment factors.

Besides TmrA, strain 8M expressed other RdhA proteins when grown with a single-electron acceptor. RdhA 260084 was not detected in cultures grown with 1,1,2-TCA, but it was produced abundantly with TCM and reached its maximum relative abundance in slices with the highest dechlorinating activity against TCM and 1,1,2-TCA (Figures 2A and S4A). In the cultures grown with TCM, RdhA 260084 clustered with the dehalogenating activity of TCM in both replicates and this interaction is even more evident when we included more proteins in the analysis (Figure S6). Despite these consistent co-migration patterns, the involvement of RdhA 260084 in TCM dechlorination is unlikely because the abundance of RdhA 260084 was two orders of magnitude lower than that of TmrA, and RdhA 260084 is almost identical (99.78% amino acid sequence identity) to the RdhA encoded in the genome of *Deh. restrictus* strain PER-K23 strain that cannot grow with TCM. Interestingly, the membrane anchor RdhB 260083 was solely detected in cells cultured with TCM as observed for its syntenic RdhA 260084. This also suggests an interaction between the RdhA and its associated RdhB protein.

The architecture of the respiratory chain in *Dehalobacter* sp. strain 8M

The predicted amino acid sequence of TmrA without the TAT-leader peptide has a calculated molecular mass of 44.4 kDa and the putative membrane anchor RdhB 40030 of 11.4 kDa. However, gel slices with TmrA were located between 100 and 200 kDa with the highest abundance at around 150 kDa. The maximum activity was in the same slice showing that reductive dehalogenases are not occurring as monomers. A dimerization of TmrA would not account for the observed mass of 150 kDa. A heterotetramer with $Rdh(AB)_2$ stoichiometry would have a mass of 112 kDa which might match the observed size in the gel, especially when considering that the gel positions in native gels can be shifted due to structural characteristics. However, the migration analyses in the native gels reproducibly show that RdhB co-migrates with HupC, that is, another membrane-integrated protein, indicating that RdhB was not associated anymore with RdhA proteins in the gel and therefore a heterotetramer of $Rdh(AB)_2$ can be ruled out as the protein complex in the observed active band. Another explanation for the occurrence of the RdhA protein in the 150 kDa region is that RdhA is part of a larger respiratory complex. Such a respiratory multiprotein complex has been found in *Dehalococcoides mccartyi* strain CBDB1 (Kublik et al., 2016) and *Dehalogenimonas alkenigignens* strain BRE15M (Trueba-Santiso et al., 2021). In these complexes, however, a complex iron–sulfur–molybdoprotein (CISM) acts as a scaffold or relay for electron transport between hydrogenase and reductive dehalogenase, obviating quinone involvement. In contrast to *Dehalobacter* strains, neither *Dehalococcoides* nor *Dehalogenimonas* encodes quinone biosynthesis. The main question at this point is therefore, if the *Dehalobacter* RdhA proteins are part of a larger protein complex and, if so, which specific proteins they interact with.

Cluster analyses of the distribution of relative protein abundances across replicate gel lanes of cultures grown with TCM and 1,1,2-TCA suggest the existence of three protein–protein interactions of respiratory proteins (Figure 6A).

Interaction I

HupL and HupS had identical migration patterns, indicating firm interaction (Figures 3, S5 and S6), as has

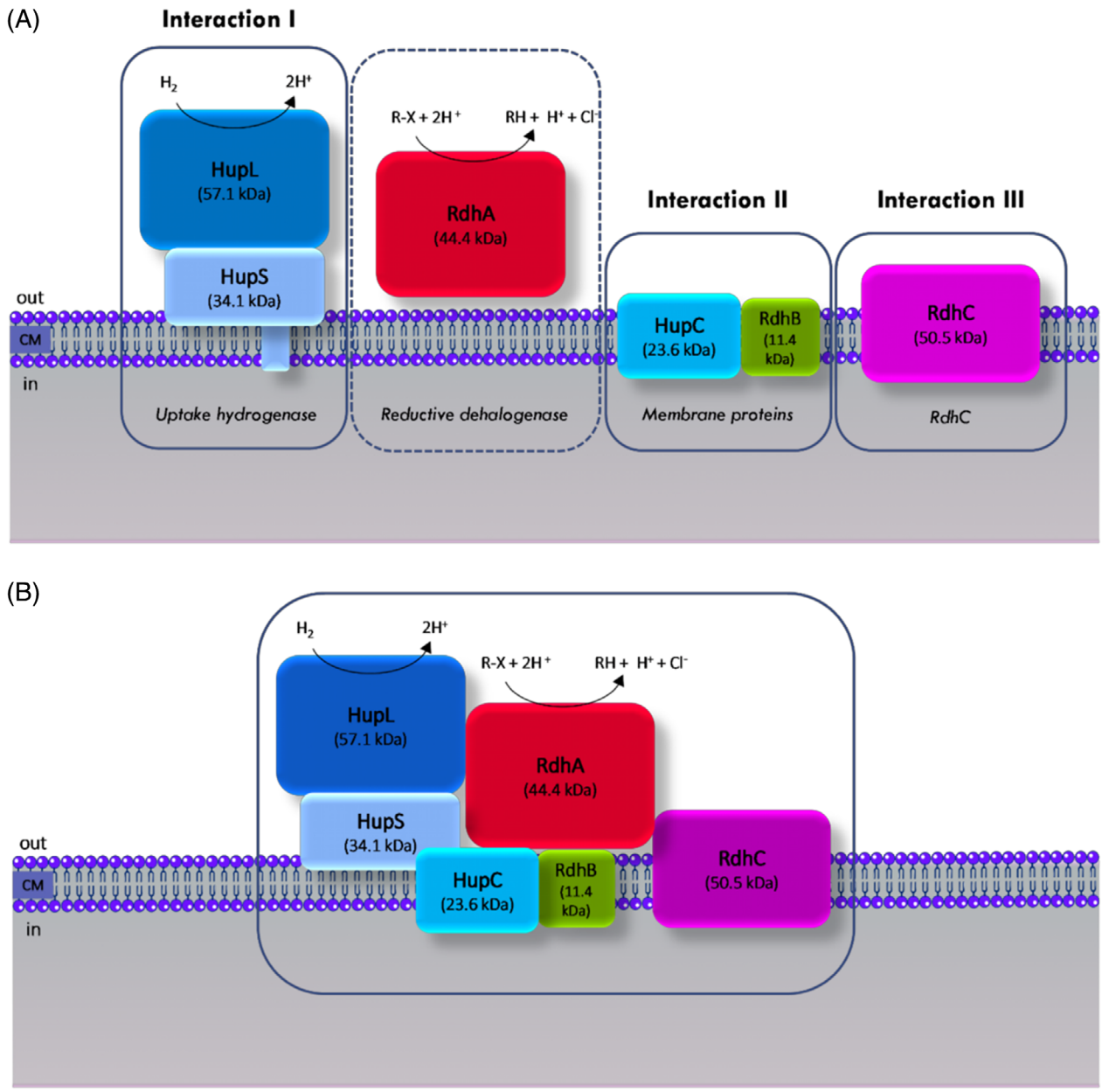

FIGURE 6 Scheme of protein interactions in *Dehalobacter* sp. strain 8M. (A) Overview of proteins and detected protein–protein interactions related to organohalide respiration. Cluster analysis indicated that RdhA 40029 (TmrA) weakly interacts with HupLS. The colour code is maintained through the figures and graphs. (B) Proposed model of an organohalide respiration complex combining the detected protein–protein interactions with the assumed interactions of HupC with HupS and of RdhA with RdhB, putatively disrupted by the detergent treatment. The roles of RdhC and quinones are elusive. HupC, b-type cytochrome; HupS, hydrogenase small subunit; HupL, hydrogenase large subunit; RdhA, reductive dehalogenase; RdhB, reductive dehalogenase anchor protein; RdhC, possibly a mixture between RdhC 40031 and RdhC 260096.

also been described for *Deh. mccartyi* strain CBDB1 and *Deh. alkenigignens* strain BRE15M (Seidel et al., 2018; Trueba-Santiso et al., 2021). In our study, both proteins had the maximum relative protein abundance in slices 5 and 6 (~127–155 kDa for TCM) and 4 and 5 (~117–149 kDa for 1,1,2-TCA). The calculated size of HupL (57.1 kDa) and HupS (34.1 kDa with removed TAT-leader peptide) together is 91.2 kDa, which is lower than observed in the gel. Together with the *b*-type cytochrome HupC (23.6 kDa, four transmembrane helices), the Hup-complex would have a size of 115 kDa, almost in the range observed in the BNE gels, but as with the RdhA, cluster analysis clearly shows the localization of HupC in other regions of the gel.

Interaction II

The relative abundance of the two membrane proteins, RdhB 40030 (11.4 kDa) and HupC 230005 (23.6 kDa), did not exhibit a distinct maximum of relative

abundance but were distributed across the protein slices up to approximately 200 kDa. Only cluster analysis revealed that the migration pattern of HupC and RdhB was very similar in all the different analyses (different cultures used or different numbers of proteins included in the analyses), suggesting that they physically interact with each other in the membrane through their hydrophobic regions.

Interaction III

The RdhC proteins 40031 (50.5 kDa) and 260096 (46.6 kDa) showed identical migration patterns with a maximum of relative protein abundance at a molecular mass of approximately 175 kDa, which is much more than the predicted molecular mass of the single proteins. The dechlorinating activity was also observed in the slice at 175 kDa, and in addition to both RdhC, the same slices showed the presence of RdhA, RdhB, HupL, HupS and HupC. This suggests that RdhC is not completely independent from the other proteins of the respiratory chain, but we cannot conclude on specific interactions. We can also not differentiate if the two RdhC proteins interact with each other or if they interact separately with other proteins. RdhB 40030 and RdhC 40031 were both detected by mass spectrometry in our studies. This is remarkable because these subunits frequently evade identification due to their small size, their low number of trypsin digestion sites, the high *m*/*z* values of tryptic peptides and the hydrophobic characteristics of the peptides (Alfan-Guzman et al., 2017a; Cimmino et al., 2022).

Our data also suggest weak interaction of RdhA with the HupLS dimer. This can be tentatively judged by evaluating the abundance distribution of RdhA and HupLS along the gel lanes in Figures 2 and S4 where the maxima consistently appear in the same or adjacent gel slices. Cluster analysis with the 60 most abundant proteins does not represent this well (Figure 3). Only when more proteins were included in the cluster analysis (Figure S6, including the 125 most abundant proteins) clustering of the RdhA proteins 40029 (TmrA) and 260094 with the HupLS dimer was evident in all four analyses (duplicate analysis with cells grown on 1,1,2-TCA or TCM). Indeed, the interaction of RdhA with HupLS (together 135.6 kDa) correlates well with the observed sizes in native gels. The HupLS dimer might partially dissociate from this interaction or interact with other proteins explaining the loose clustering. BNE is a valuable approach for analysing protein–protein interactions, but it has limitations that can lead to misinterpretation of data. Co-migration alone does not imply physical interaction, as similar-sized complexes can appear in the same protein band. However, physical interaction can explain co-migration. Weak or transient protein–protein interactions pose challenges in BNE, as the use of detergents can weaken protein associations and negatively charged Coomassie dye can disrupt fragile protein complexes. Additional techniques like immunoprecipitations or co-migration under different conditions, such as non-sized-based chromatography, can confirm protein–protein interactions (Eubel et al., 2005).

The detected protein–protein interactions constrain a model for the respiratory architecture in *Dehalobacter* strains. All detected proteins together would give a complex of 221.1 kDa (HupLS: 91.2 kDa; HupC and RdhB: 34.9 kDa, RdhC: 50.5 kDa; RdhA: 44.4 kDa), which is larger than the observed molecular mass of 100–200 kDa, where the highest dehalogenation activity was determined. Again, it must be kept in mind that the size estimation is not precise in BNE gels (Seidel et al., 2018). A possible explanation is that the membrane-integrated proteins HupC and RdhB were removed by detergent treatment resulting in a theoretical mass of 186.1 kDa (HupLS, RdhA, RdhC) or 135.6 kDa (HupLS, RdhA). A removal of HupC and RdhB from the protein complex would probably also weaken the overall integrity of a complex assuming in vivo interactions of HupLS with HupC and RdhA with RdhB (Bommer et al., 2014).

The role of RdhC

The overall structure formed by the single protein RdhC is similar to structures formed by three protein subunits in other organisms, that is, Nqr (NADH: quinone oxidoreductase) of *Vibrio cholerae* (Steuber et al., 2014) and Rnf (ferredoxin: NAD oxidoreductase) of *Clostridium tetanomorphum* (Vitt et al., 2022). Both complexes participate in membrane potential coupled redox reactions (Reyes-Prieto et al., 2014). The exoplasmic FMN-binding domain of RdhC is homologous to NqrC and RnfG, whereas the architecture of the transmembrane helices in the C-terminal membrane-integrated half of RdhC is strikingly similar to the membrane-integrated subunit twins NqrDE and RnfEA. These subunit twins of NqrDE and RnfEA form symmetrical dimers within the membrane, where the monomers are rotated by 180°. Four central helices of NqrDE or RnfEA form a core structure, where a [2Fe-2S] cluster is coordinated by four cysteine residues (Fritz, 2023; Kishikawa et al., 2022; L. Zhang & Einsle, 2022), and not a mononuclear iron atom as has been previously described (Steuber et al., 2014; Vitt et al., 2022). Two cysteine residues originate from the core helices of one subunit each of NqrDE or RnfEA. The [2Fe-2S] cluster is located in the middle of the membrane plane in the Nqr and Rnf complexes, possibly enabling the conduction of electrons through the membrane (Kishikawa et al., 2022; Steuber et al., 2014; Vitt et al., 2022). The C-terminal part of

RdhC has the same architecture and four cysteine residues within one polypeptide chain forming a cavity for putative metal binding. The strong structural similarity suggests that indeed a [2Fe-2S] cluster is bound to RdhC and not a [4Fe-4S] cluster as predicted by MetalPredator. Experimental evidence is necessary to test this hypothesis. Together, the observed similarities to Nqr and Rnf complexes suggest that RdhC could form an electron path through the membrane with a central [2Fe-2S] cluster in the membrane plane, electrically connected with an exoplasmic FMN unit. The participation of RdhC in organohalide respiration has been hypothesized before based on its co-location in the reductive dehalogenase operon and the presence of an FMN-binding motif (Buttet et al., 2018; Cimmino et al., 2022). The integration of this protein in the organohalide respiration chain, however, is not clear. One possibility for a biochemical role of RdhC is the coupling of electron flow from haeme groups of HupC to the reductive dehalogenase to proton or sodium transport across the membrane. Then RdhC would have a similar role as OmeAB might have in the dehalogenase complex of *Dehalococcoidia* (Kublik et al., 2016). Such involvement of RdhC would obviate the involvement of quinones in electron transport in *Dehalobacter* and resolve the paradox of how electrons can be transferred to the low-potential corrinoid cluster via a high-potential quinone pool. Also, this may give an explanation of why some *Dehalobacter* strains are capable of reductive dehalogenation of chlorobenzenes, chloroanilines, chlorophenols and chlorodioxins otherwise only described for members of the *Dehalococcoidia* (Alfan-Guzman et al., 2017a; Nelson et al., 2014; Wang et al., 2014; S. Zhang, Wondrousch, et al., 2017). However, both our complexome data and stoichiometric analysis of RdhC versus RdhAB (Cimmino et al., 2022) suggest that RdhC is not directly involved, although we cannot rule out that the complexome approach misses important interactions. Moreover, previous biochemical experiments have indicated the involvement of quinones in the reductive dehalogenation of perchloroethene by *Deh. restrictus* (Schumacher & Holliger, 1996). A resolution to this conundrum could be the existence of different electron paths for different halogenated electron acceptors in *Dehalobacter* strains. At present, the specific role of RdhC in this process remains elusive.

AUTHOR CONTRIBUTIONS

Jesica M. Soder-Walz: Conceptualization (supporting); data curation (equal); formal analysis (equal); investigation (lead); methodology (lead); software (equal); writing—original draft (lead); writing—review and editing (equal). **Kenneth Wasmund:** Data curation (equal); formal analysis (equal); methodology (equal); software (equal); writing—review and editing (equal). **Darja Deobald:** Formal analysis (equal); software (equal); writing—original draft (supporting); writing—review and editing (equal). **Teresa Vicent:** Resources (equal); validation (equal); writing—review and editing (equal). **Lorenz Adrian:** Conceptualization (supporting); data curation (supporting); resources (equal); supervision (supporting); writing—original draft (supporting); writing—review and editing (equal). **Ernesto Marco-Urrea:** Conceptualization (lead); data curation (equal); formal analysis (equal); funding acquisition (lead); project administration (lead); supervision (lead); writing—original draft (supporting); writing–review and editing (equal).

ACKNOWLEDGEMENT

Protein mass spectrometry was performed at the Centre for Chemical Microscopy (ProVIS) at the Helmholtz Centre for Environmental Research—UFZ. Open Access funding enabled and organized by Projekt DEAL.

FUNDING INFORMATION

This work was funded by MCIN/AEI/10.13039/501100011033 (grant ref. PID2019-103989RB-I00) and partially supported by the Generalitat de Catalunya (Consolidated Research Group 2021-SGR-01008).

CONFLICT OF INTEREST STATEMENT

The authors declare no conflicts of interest.

DATA AVAILABILITY STATEMENT

Data supporting the findings are available in the supplementary material. The genome sequence and annotations are publicly available on the MicroScope platform: https://mage.genoscope.cns.fr/microscope/mage/viewer.php?O_id=14849. The genome sequence was also submitted to NCBI under the BioProject PRJNA922222: https://www.ncbi.nlm.nih.gov/bioproject/PRJNA922222.

ORCID

Jesica M. Soder-Walz https://orcid.org/0000-0002-5253-9898
Kenneth Wasmund https://orcid.org/0000-0001-6706-7291
Darja Deobald https://orcid.org/0000-0003-0882-5499
Teresa Vicent https://orcid.org/0000-0002-6547-7358
Lorenz Adrian https://orcid.org/0000-0001-8205-0842
Ernest Marco-Urrea https://orcid.org/0000-0002-8033-6553

REFERENCES

Adrian, L., Hansen, S.K., Fung, J.M., Görisch, H. & Zinder, S.H. (2007) Growth of *Dehalococcoides* strains with chlorophenols as electron acceptors. *Environmental Science & Technology*, 41, 2318–2323.

Agency for Toxic Substances and Disease Registry (ATSDR). (2022) Priority list of hazardous substances. Available from: https://www.atsdr.cdc.gov/spl/#2022spl [Accessed 18 January 2023].

Alfan-Guzman, R., Ertan, H., Manefield, M. & Lee, M. (2017a) Isolation and characterization of *Dehalobacter* sp. strain TeCB1 including identification of *tcbA*: a novel tetra- and trichlorobenzene reductive dehalogenase. *Frontiers in Microbiology*, 8, 558.

Alfan-Guzman, R., Ertan, H., Manefield, M. & Lee, M. (2017b) Genome sequence of *Dehalobacter* sp. strain TeCB1, able to respire chlorinated benzenes. *Genome Announcements*, 5. https://doi.org/10.1128/genomea.01681-16

Aziz, R.K., Bartels, D., Best, A.A., DeJongh, M., Disz, T., Edwards, R.A. et al. (2008) The RAST server: rapid annotations using subsystems technology. *BMC Genomics*, 9, 75.

Bali, S., Lawrence, A.D., Lobo, S.A., Saraiva, L.M., Golding, B.T., Palmer, D.J. et al. (2011) Molecular hijacking of siroheme for the synthesis of heme and d_1 heme. *Proceedings of the National Academy of Sciences*, 108, 18260–18265.

Bankevich, A., Nurk, S., Antipov, D., Gurevich, A.A., Dvorkin, M., Kulikov, A.S. et al. (2012) SPAdes: a new genome assembly algorithm and its applications to single-cell sequencing. *Journal of Computational Biology*, 19, 455–477.

Blázquez-Pallí, N., Rosell, M., Varias, J., Bosch, M., Soler, A., Vicent, T. et al. (2019) Integrative isotopic and molecular approach for the diagnosis and implementation of an efficient in-situ enhanced biological reductive dechlorination of chlorinated ethenes. *Water Research*, 167, 115106.

Bommer, M., Kunze, C., Fesseler, J., Schubert, T., Diekert, G. & Dobbek, H. (2014) Structural basis for organohalide respiration. *Science*, 346, 455–458.

Buttet, G.F., Willemin, M.S., Hamelin, R., Rupakula, A. & Maillard, J. (2018) The membrane-bound c subunit of reductive dehalogenases: topology analysis and reconstitution of the FMN-binding domain of PceC. *Frontiers in Microbiology*, 9, 755.

Cimmino, L., Schmid, A.W., Holliger, C. & Maillard, J. (2022) Stoichiometry of the gene products from the tetrachloroethene reductive dehalogenase operon *pceABCT*. *Frontiers in Microbiology*, 13, 838026.

Ding, C., Zhao, S. & He, J. (2014) A *Desulfitobacterium* sp. strain PR reductively dechlorinates both 1,1,1-trichloroethane and chloroform. *Environmental Microbiology*, 16, 3387–3397.

Duret, A., Holliger, C. & Maillard, J. (2012) The physiological opportunism of *Desulfitobacterium hafniense* strain TCE1 towards organohalide respiration with tetrachloroethene. *Applied and Environmental Microbiology*, 78, 6121–6127.

Edgar, R. (2004) MUSCLE: multiple sequence alignment with high accuracy and high throughput. *Nucleic Acids Research*, 32, 1792–1797.

Eubel, H., Braun, H.-P. & Millar, A. (2005) Blue-native PAGE in plants: a tool in analysis of protein-protein interactions. *Plant Methods*, 1, 11.

Fritz, G. (2023) A [2Fe-2S] cluster is bound between the NqrD and NqrE subunits of the NQR complex of *Vibrio cholerae*. *SPP1927 Meeting*, personal communication on 04.05.2023. Universität Hohenheim.

Geer, L.Y., Domrachev, M., Lipman, D.J. & Bryant, S.H. (2002) CDART: protein homology by domain architecture. *Genome Research*, 12, 1619–1623.

Heckel, B., Phillips, E., Edwards, E., Sherwood Lollar, B., Elsner, M., Manefield, M.J. et al. (2019) Reductive dehalogenation of trichloromethane by two different *Dehalobacter restrictus* strains reveal opposing dual element isotope effects. *Environmental Science & Technology*, 53, 2332–2343.

Hug, L.A., Maphosa, F., Leys, D., Löffler, F.E., Smidt, H., Edwards, E.A. et al. (2013) Overview of organohalide-respiring bacteria and a proposal for a classification system for reductive dehalogenases. *Philosophical Transactions of the Royal Society B: Biological Sciences*, 368, 20120322.

Hölscher, T., Krajmalnik-Brown, R., Ritalahti, K., von Wintzingerode, F., Görisch, H., Löffler, F. et al. (2004) Multiple nonidentical reductive-dehalogenase-homologous genes are common in *Dehalococcoides*. *Applied and Environmental Microbiology*, 70, 5290–5297.

Jugder, B.-E., Bohl, S., Lebhar, H., Healey, R.D., Manefield, M., Marquis, C.P. et al. (2017) A bacterial chloroform reductive dehalogenase: purification and biochemical characterization. *Microbial Biotechnology*, 10, 1640–1648.

Jugder, B.-E., Ertan, H., Bohl, S., Lee, M., Marquis, C.P. & Manefield, M. (2016) Organohalide respiring bacteria and reductive dehalogenases: key tools in organohalide bioremediation. *Frontiers in Microbiology*, 7, 249.

Jugder, B.-E., Ertan, H., Lee, M., Manefield, M. & Marquis, C.P. (2015) Reductive dehalogenases come of age in biological destruction of organohalides. *Trends in Biotechnology*, 33, 595–610.

Kishikawa, J.-I., Ishikawa, M., Masuya, T., Murai, M., Kitazumi, Y., Butler, N.L. et al. (2022) Cryo-EM structures of Na+-pumping NADH-ubiquinone oxidoreductase from *Vibrio cholerae*. *Nature Communications*, 13, 4082.

Kräutler, B., Fieber, W., Ostermann, S., Fasching, M., Ongania, K.-H., Gruber, K. et al. (2003) The cofactor of tetrachloroethene reductive dehalogenase of *Dehalospirillum multivorans* is norpseudo-B_{12}, a new type of a natural corrinoid. *Helvetica Chimica Acta*, 86, 3698–3716.

Kublik, A., Deobald, D., Hartwig, S., Schiffmann, C.L., Andrades, A., von Bergen, M. et al. (2016) Identification of a multi-protein reductive dehalogenase complex in *Dehalococcoides mccartyi* strain CBDB1 suggests a protein-dependent respiratory electron transport chain obviating quinone involvement. *Environmental Microbiology*, 18, 3044–3056.

Kühner, M., Haufschildt, K., Neumann, A., Storbeck, S., Streif, J. & Layer, G. (2014) The alternative route to heme in the methanogenic archaeon *Methanosarcina barkeri*. *Archaea*, 2014, 327637.

Layer, G. (2021) Heme biosynthesis in prokaryotes. *Biochimica et Biophysica Acta (BBA)—Molecular Cell Research*, 1868, 118861.

Maillard, J. & Holliger, C. (2016) The genus *Dehalobacter*. In: Adrian, L. & Löffler, F.E. (Eds.) *Organohalide-respiring bacteria*. Berlin, Heidelberg: Springer Berlin Heidelberg, pp. 153–171.

Maillard, J., Genevaux, P. & Holliger, C. (2011) Redundancy and specificity of multiple trigger factor chaperones in *Desulfitobacteria*. *Microbiology*, 157, 2410–2421.

Mirdita, M., Schütze, K., Moriwaki, Y., Heo, L., Ovchinnikov, S. & Steinegger, M. (2022) ColabFold: making protein folding accessible to all. *Nature Methods*, 19, 679–682.

Nelson, J.L., Jiang, J. & Zinder, S.H. (2014) Dehalogenation of chlorobenzenes, dichlorotoluenes, and tetrachloroethene by three *Dehalobacter* spp. *Environmental Science & Technology*, 48, 3776–3782.

Padilla-Crespo, E., Yan, J., Swift, C., Wagner, D.D., Chourey, K., Hettich, R.L. et al. (2014) Identification and environmental distribution of *dcpA*, which encodes the reductive dehalogenase catalyzing the dichloroelimination of 1,2-dichloropropane to propene in organohalide-respiring *Chloroflexi*. *Applied and Environmental Microbiology*, 80, 808–818.

Papadopoulos, J.S. & Agarwala, R. (2007) COBALT: constraint-based alignment tool for multiple protein sequences. *Bioinformatics*, 23, 1073–1079.

Parks, D.H., Imelfort, M., Skennerton, C.T., Hugenholtz, P. & Tyson, G.W. (2015) CheckM: assessing the quality of microbial genomes recovered from isolates, single cells, and metagenomes. *Genome Research*, 25, 1043–1055.

Phillips, E., Bulka, O., Picott, K., Kümmel, S., Edwards, E.A., Nijenhuis, I. et al. (2022) Investigation of active site amino acid influence on carbon and chlorine isotope fractionation during reductive dechlorination. *FEMS Microbiology Ecology*, 98, fiac072.

Reyes-Prieto, A., Barquera, B. & Juárez, O. (2014) Origin and evolution of the sodium-pumping NADH: ubiquinone oxidoreductase. *PLoS One*, 9, e96696.

Richter, M., Rosselló-Móra, R., Oliver Glöckner, F. & Peplies, J. (2016) JSpeciesWS: a web server for prokaryotic species circumscription based on pairwise genome comparison. *Bioinformatics*, 32, 929–931.

Rothery, R.A., Workun, G.J. & Weiner, J.H. (2008) The prokaryotic complex iron–sulfur molybdoenzyme family. *Biochimica et Biophysica Acta—Biomembranes*, 1778, 1897–1929.

Rupakula, A., Kruse, T., Boeren, S., Holliger, C., Smidt, H. & Maillard, J. (2013) The restricted metabolism of the obligate organohalide respiring bacterium *Dehalobacter restrictus*: lessons from tiered functional genomics. *Philosophical Transactions of the Royal Society B: Biological Sciences*, 368, 20120325.

Sayers, E.W., Bolton, E.E., Brister, J.R., Canese, K., Chan, J., Comeau, D.C. et al. (2022) Database resources of the National Center for Biotechnology Information. *Nucleic Acids Research*, 50, D20–D26.

Schrödinger, L. & DeLano, W. (2020) PyMOL. Available from: http://wwwpymolorg/pymol

Schubert, M., Lindgreen, S. & Orlando, L. (2016) AdapterRemoval v2: rapid adapter trimming, identification, and read merging. *BioMed Central Research Notes*, 9, 1–7.

Schumacher, W. & Holliger, C. (1996) The proton/electron ratio of the menaquinone-dependent electron tansport from dihydrogen to tetrachloroethene in '*Dehalobacter restrictus*'. *Journal of Bacteriology*, 178, 2328–2333.

Seidel, K., Kühne, J. & Adrian, L. (2018) The complexome of *Dehalococcoides mccartyi* reveals its organohalide respiration-complex is modular. *Frontiers in Microbiology*, 9, 1130.

Soder-Walz, J.M., Torrentó, C., Algora, C., Wasmund, K., Cortés, P., Soler, A. et al. (2022) Trichloromethane dechlorination by a novel *Dehalobacter* sp. strain 8M reveals a third contrasting C and Cl isotope fractionation pattern within this genus. *Science of the Total Environment*, 813, 152659.

Steuber, J., Vohl, G., Casutt, M.S., Vorburger, T., Diederichs, K. & Fritz, G. (2014) Structure of the *V. cholerae* Na^+-pumping NADH:quinone oxidoreductase. *Nature*, 516, 62–67.

Tamura, K., Stecher, G. & Kumar, S. (2021) MEGA11: molecular evolutionary genetics analysis version 11. *Molecular Biology and Evolution*, 38, 3022–3027.

Tang, S. & Edwards, E.A. (2013) Identification of *Dehalobacter* reductive dehalogenases that catalyse dechlorination of chloroform, 1,1,1-trichloroethane and 1,1-dichloroethane. *Philosophical Transactions of the Royal Society B: Biological Sciences*, 368, 20120318.

Teufel, F., Almagro Armenteros, J.J., Johansen, A.R., Gíslason, M.H., Pihl, S.I., Tsirigos, K.D. et al. (2022) SignalP 6.0 predicts all five types of signal peptides using protein language models. *Nature Biotechnology*, 40, 1023–1025.

Trifinopoulos, J., Nguyen, L.-T., von Haeseler, A. & Minh, B.Q. (2016) W-IQ-TREE: a fast online phylogenetic tool for maximum likelihood analysis. *Nucleic Acids Research*, 44, W232–W235.

Trueba-Santiso, A., Parladé, E., Rosell, M., Lliros, M., Mortan, S.H., Martínez-Alonso, M. et al. (2017) Molecular and carbon isotopic characterization of an anaerobic stable enrichment culture containing *Dehalobacterium* sp. during dichloromethane fermentation. *Science of the Total Environment*, 581, 640–648.

Trueba-Santiso, A., Wasmund, K., Soder-Walz, J.M., Marco-Urrea, E. & Adrian, L. (2021) Genome sequence, proteome profile, and identification of a multiprotein reductive dehalogenase complex in *Dehalogenimonas alkenigignens* strain BRE15M. *Journal of Proteome Research*, 20, 613–623.

Valasatava, Y., Rosato, A., Banci, L. & Andreini, C. (2016) MetalPredator: a web server to predict iron–sulfur cluster binding proteomes. *Bioinformatics*, 32, 2850–2852.

Vallenet, D., Calteau, A., Dubois, M., Amours, P., Bazin, A., Beuvin, M. et al. (2020) MicroScope: an integrated platform for the annotation and exploration of microbial gene functions through genomic, pangenomic and metabolic comparative analysis. *Nucleic Acids Research*, 48, D579–D589.

Vitt, S., Prinz, S., Eisinger, M., Ermler, U. & Buckel, W. (2022) Purification and structural characterization of the Na^+-translocating ferredoxin: NAD^+ reductase (Rnf) complex of *Clostridium tetanomorphum*. *Nature Communications*, 13, 6315.

Wang, S., Qiu, L., Liu, X., Xu, G., Siegert, M., Lu, Q. et al. (2018) Electron transport chains in organohalide-respiring bacteria and bioremediation implications. *Biotechnology Advances*, 36, 1194–1206.

Wang, S., Zhang, W., Yang, K.-L. & He, J. (2014) Isolation and characterization of a novel *Dehalobacter* species strain TCP1 that reductively dechlorinates 2,4,6-trichlorophenol. *Biodegradation*, 25, 313–323.

Wong, Y.K., Holland, S.I., Ertan, H., Manefield, M. & Lee, M. (2016) Isolation and characterization of *Dehalobacter* sp. strain UNSWDHB capable of chloroform and chlorinated ethane respiration. *Environmental Microbiology*, 18, 3092–3105.

Yang, M.I., Previdsa, M., Edwards, E.A. & Sleep, B.E. (2020) Two distinct *Dehalobacter* strains sequentially dechlorinate 1,1,1-trichloroethane and 1,1-dichloroethane at a field site treated with granular zero valent iron and guar gum. *Water Research*, 186, 116310.

Zhang, C., Freddolino, P.L. & Zhang, Y. (2017) COFACTOR: improved protein function prediction by combining structure, sequence and protein–protein interaction information. *Nucleic Acids Research*, 45, W291–W299.

Zhang, L. & Einsle, O. (2022) Architecture of the NADH:ferredoxin oxidoreductase RNF that drives biological nitrogen fixation. *bioRxiv* 2022.2007.2008.499327.

Zhang, S., Wondrousch, D., Cooper, M., Zinder, S.H., Schüürmann, G. & Adrian, L. (2017) Anaerobic dehalogenation of chloroanilines by *Dehalococcoides mccartyi* strain CBDB1 and *Dehalobacter* strain 14DCB1 via different pathways as related to molecular electronic structure. *Environmental Science & Technology*, 51, 3714–3724.

Zhao, S., Rogers, M.J. & He, J. (2017) Microbial reductive dehalogenation of trihalomethanes by a *Dehalobacter*-containing co-culture. *Applied Microbiology and Biotechnology*, 101, 5481–5492.

Zimmermann, L., Stephens, A., Nam, S.-Z., Rau, D., Kübler, J., Lozajic, M. et al. (2018) A completely reimplemented MPI bioinformatics toolkit with a new HHpred server at its core. *Journal of Molecular Biology*, 430, 2237–2243.

SUPPORTING INFORMATION

Additional supporting information can be found online in the Supporting Information section at the end of this article.

How to cite this article: Soder-Walz, J.M., Wasmund, K., Deobald, D., Vicent, T., Adrian, L. & Marco-Urrea, E. (2023) Respiratory protein interactions in *Dehalobacter* sp. strain 8M revealed through genomic and native proteomic analyses. *Environmental Microbiology*, 1–17. Available from: https://doi.org/10.1111/1462-2920.16464